Am J Transl Res 2026;18(2):1037-1052
www.ajtr.org /ISSN:1943-8141/AJTR0161437

Original Article

GSDME-mediated pyroptosis is essential for the chemotherapeutic effects achieved by combined treatment of temsirolimus and 5-fluorouracil in ovarian carcinoma cells

Zhenbo Chen[1], Mingxia Ye[1*], Chenglei Gu[1*], Na Wen[2*], Nan Wang[1*], Yuanguang Meng[1]

[1]Department of Gynecology and Obstetrics, People's Liberation Army (PLA) Medical School, Chinese PLA General Hospital, Beijing 100853, China; [2]Department of Gynecology and Obstetrics, The Eighth Medical Center of The PLA, Beijing 100039, China. [*]Equal contributors.

Received October 24, 2024; Accepted December 26, 2025; Epub February 15, 2026; Published February 28, 2026

Abstract: Objectives: The expression of GSDMD and GSDME in ovarian cancerous tissues, adjacent tissues, and cancer cell lines remain poorly characterized. The contribution of pyroptosis to the synergistic therapeutic effects of PI3K-AKT-mTOR inhibitors and cell cycle inhibitors in ovarian carcinoma is unknown. Method: GSDME and GSDMD expression were quantified in ovarian cancer tissues, adjacent tissues, and cancer cell lines. The cytotoxic effects of temsirolimus (an PI3K-AKT-mTOR inhibitor) and 5-fluorouracil (5-FU, a cell cycle inhibitor) were assessed. Results: Both GSDMD and GSDME were detected in ovarian cancer tissues and adjacent tissues. However, the N-terminals of GSDME and GSDMD were only expressed in cancerous tissues, with the GSDME-N terminal being particularly prominent. Similarly, in ovarian cancer cell lines, only GSDME-N terminal was increased when treated by temsirolimus and 5-FU, together with significantly suppressed cell proliferation. Synergistic treatment with temsirolimus and 5-FU further reduced cancer cell viability and enhanced pyroptosis by upregulating GSDME-N terminal expression. RNA interference confirmed that GSDME-mediated pyroptosis is essential for the cytotoxic effects of monotherapy and combination chemotherapy. 5-FU fails to induce complete conversion of pyroptosis to ferroptosis when combined with temsirolimus, even at extremely high concentrations. The drug combination also promoted apoptosis and ferroptosis, which were significantly attenuated by N-acetyl-L-cysteine (NAC). Conclusion: GSDME is the principal executor of spontaneous pyroptosis in ovarian cancer tissues. In chemotherapy employing cell cycle-targeting agents or PI3K-AKT-mTOR pathway inhibitors (alone or in combination) is beneficial, and pyroptosis is an indispensable cell death mechanism. Reactive oxygen species act as a nodal regulator orchestrating pyroptosis, apoptosis, and ferroptosis.

Keywords: GSDME, pyroptosis, temsirolimus, 5-FU, ovarian carcinoma

Introduction

Ovarian cancer ranks as the fourth leading cause of cancer-related mortality among women [1]. While chemotherapy remains a cornerstone of ovarian cancer treatment, its efficacy is often limited, necessitating the development of more effective therapeutic approaches. Traditionally, apoptosis has been regarded as the primary form of regulated programmed cell death and serves as the predominant mechanism by which cancer cells are sensitized to chemotherapy and radiotherapy [2]. However, pyroptosis, a recently elucidated form of inflammatory programmed cell death, is emerging as a critical mechanisms for cancer cell death, and it plays an important role in improving chemotherapy effects and the 5-year survival rate of ovarian cancer patients [3]. Unlike apoptosis, pyroptosis is characterized by the formation of pores in the cell membrane, resulting in cell lysis and the release of pro-inflammatory signals. This mechanism not only promotes direct tumor cell death, but can also overcome resistance to apoptosis-associated drugs in ovarian cancer [4, 5]. Furthermore, pyroptosis and tu-

https://doi.org/10.62347/TJWX5574

Table 1. Abbreviations

Abbreviations	Full length name
GSDME	Gasdermin E
GSDMD	Gasdermin D
mTOR	Mammalian target of rapamycin
5-FU	5-Fluorouracil
ICIs	Immune checkpoint inhibitors
PI3K	Phosphatidylinositol 3-kinase
ROS	Reactive oxygen species
DMEM	Dulbecco's Modified Eagle Medium
HMGB1	High-mobility group box 1 protein
FBS	Fetal bovine serum
PBS	Phosphate-buffered saline
siRNA	Small interfering RNA
CCK-8	Cell Counting Kit-8
MDA	Malondialdehyde
NAC	N-acetyl-L-cysteine
GSH	Glutathione
PARP	Poly (ADP-ribose) polymerase
RSL3	Ras-selective lethal 3
GPX4	Glutathione peroxidase 4
ACSL4	Acyl-CoA synthetase long-chain family member 4
P-S6	Phosphorylated ribosomal protein S6

mor immunotherapy exhibit synergistic potential. Pyroptotic cells release damage-associated molecular patterns (DAMPs), which stimulate adaptive immune responses and potentiate the efficacy of immune checkpoint inhibitors (ICIs) (**Table 1**) [6]. Notably, emerging evidence suggests ICIs may attain optimal therapeutic outcomes only when combined with pyroptosis induction [7], highlighting the importance of pyroptosis in anti-tumor therapy.

Combination chemotherapy is extensively utilized in clinical oncology to address the inherent resistance of tumor cells to single-agent treatment modalities [8, 9]. Cell cycle arresting drugs, such as 5-fluorouracil (5-FU) and platinum-based compounds, constitute the foundational elements of many chemotherapy regimens. Additionally, the PI3K (phosphoinositide 3-kinase)-AKT (protein kinase B)-mTOR (mammalian target of rapamycin) signaling pathway is frequently hyperactivated in ovarian cancer, and serves as a critical driver of chemoresistance [10]. Reactive oxygen species (ROS), especially lipid peroxidation, are primarily neutralized by glutathione peroxidase 4 (GPX4). Inhibition of GPX4 diminishes cellular antioxidant defenses, leading to the accumulation of ROS and ultimately inducing cell death via ferroptosis. Mutations in the PI3K-AKT-mTOR pathway further upregulate proteins involved in lipid biosynthesis, whereas pharmacological blockade of this pathway attenuates excessive lipid production, thereby sensitizing cells to ferroptosis. Given the central role of mTOR signaling in regulating tumor cell sensitivity to anticancer therapies, the combination of mTOR inhibitors with traditional cell cycle - targeting agents has emerged as a rational strategy in clinical trials [11]. Temsirolimus (Synonyms: CCI-779), an mTOR inhibitor, has been used in a variety of clinical trials. The combination of temsirolimus and other anti-cancer drugs have shown good tolerance and clinical efficacy in the treatment of ovarian cancer [12-14]. In this study, we sought to elucidate the role of GSDME-mediated pyroptosis in the synergistic anti-tumor effects observed when combining 5-FU and temsirolimus in ovarian cancer cell lines.

GSDMD and GSDME are pivotal mediators of pyroptosis and belong to the gasdermin protein family. Upon proteolytic cleavage, these proteins release their N-terminal domains, which subsequently oligomerize and form pores within the cell membrane, an essential hallmark of pyroptotic cell death. Pyroptosis can be initiated via two primary pathways: (1) the canonical pathway, where caspase-1 (or caspase-4/5 in humans; caspase-11 in mice) cleaves GSDMD [15], and (2) the non-canonical pathway, in which activation of caspase-3 or caspase-7 leads to GSDME cleavage. Both pathways compromise membrane integrity, resulting in lytic cell death and the release of pro-inflammatory cytokines.

Although pyroptosis plays a critical role in the combined use of temsirolimus and cell cycle inhibitors, several questions remain regarding the specific mechanisms and therapeutic sig-

nificance of pyroptosis in ovarian cancer cell response to chemotherapy. A primary question is to directly characterize the expression of GSDMD and GSDME, as well as their activated N-terminal fragments, in ovarian cancer tissues, adjacent normal tissues, and ovarian cancer cell lines. To date, the direct presence and functional activation of gasdermin family members in ovarian cancer under chemotherapy remains insufficiently investigated. For example, one study reported upregulation of GSDMD in ovarian cancer based solely on bioinformatic analyses [16]. In another study, lncRNA GAS5 was found to induce inflammasome formation and promote pyroptosis through GSDMD, yet pyroptosis was assessed by measuring caspase-1, procaspase-1, IL-1β, pro-IL-1β, IL-18, and pro-IL-18 protein levels using Western blot, rather than direct morphological assessment [17]. Further, emerging research indicates that lncRNA HOTTIP acts as an oncogene in ovarian cancer, with its suppression resulting in the induction of pyroptosis and concomitant inhibition of tumor progression; however, in this study, pyroptosis was inferred from increased IL-18, IL-1β, and caspase-1 activation, without evaluation of characteristic features such as cell swelling or pore formation [18]. Much of the existing literature on pyroptosis in ovarian cancer has focused on GSDMD. For instance, 2-(naphthoyl) ethyltrimethylammonium iodide (a-NETA) was shown to induce pyroptosis via the caspase-4/GSDMD pathway [19]. Only few studies have reported on the role of GSDME in ovarian cancer, with bioinformatic analyses suggesting altered GSDME expression in ovarian tumors [16, 20]. Experimental data from Zhang et al. demonstrated that nobiletin increases ROS production and autophagy, promoting cleavage of both GSDMD and GSDME [21]. Similarly, Liang et al. found that osthole suppresses ovarian carcinoma cell growth in part by inducing GSDME-dependent pyroptosis [22]. Notably, neither nobiletin nor osthole are standard chemotherapeutic agents. Collectively, these observations underscore the need for direct investigation of whether GSDME or GSDMD functions as the predominant mediator of pyroptosis in ovarian cancer cells subjected to conventional chemotherapy, which remains critical for the development of refined therapeutic strategies. Furthermore, although previous studies have identified the caspase-3/7/GSDME axis as a canonical pathway mediating pyroptosis, the specific contributions of individual caspases to GSDME cleavage in ovarian cancer cells undergoing chemotherapy remain to be elucidated. In this study, we employed siRNA-mediated knockdown of caspase-3 and caspase-7 to dissect their respective roles in mediating GSDME activation and pyroptotic cell death under chemotherapeutic conditions.

Secondly, we aimed to assess whether the combination of an mTOR inhibitor (temsirolimus) and a DNA replication inhibitor (5-FU) synergistically enhances therapeutic efficacy against ovarian cancer cell lines by inducing pyroptosis. Specifically, this study sought to elucidate the functional contribution of pyroptosis to the increased cytotoxicity observed with this combinatorial regimen, as well as to identify the specific gasdermin (GSDM) family member(s) acting as key executors of pyroptosis in response to dual drug treatment.

Thirdly, apoptosis is well-established as a principal cell death pathway in antitumor therapy [13]. Prior studies have shown that combinations of PI3K-Akt-mTOR pathway inhibitors and platinum-based chemotherapeutics synergistically increase apoptotic rates in ovarian cancer cells [10, 23, 24]. Moreover, recent research indicates that DNA replication inhibitors elicit a multimodal cell death response in ovarian carcinoma cell lines, encompassing pyroptosis, apoptosis, and ferroptosis [25, 26]. While the mechanisms underlying apoptosis are thoroughly characterized, the roles and relative contributions of non-apoptotic cell death modalities, particularly pyroptosis, in mediating the efficacy of combination chemotherapy remain insufficiently understood and warrant further investigation.

Finally, oxidative stress is recognized as a major inducer of pyroptosis, apoptosis, and ferroptosis across a range of pathological conditions [27]. Reactive oxygen species (ROS), a key mediator of lipid peroxidation, plays a pivotal role in the mechanisms underlying the efficacy of both single-agent and combination cancer therapies. Numerous studies have shown that agents modulating oxidative stress metabolism can preferentially eliminate cancer cells by increasing ROS or lipid peroxide levels to cytotoxic thresholds [28]. Recent preclinical investigations have highlighted synergistic therapeutic strategies targeting the mTOR pathway.

Temsirolimus, an ATP-competitive inhibitor of mTORC1, perturbs cellular redox homeostasis by impeding autophagic clearance of ROS and phospholipid hydroperoxides [29]. When used in combination with RSL3, a specific inhibitor of GPX4, this dual-targeting approach results in pronounced accumulation of lipid peroxides and induces ferroptosis, a regulated, iron-dependent non-apoptotic cell death characterized by oxidative membrane damage. In breast and prostate cancer xenograft models, simultaneous inhibition of mTOR and GPX4 achieved near-complete tumor regression, with mechanistic studies confirming ferroptosis as the primary mode of cell death [29]. DNA replication inhibitors such as 5-FU also exert anti-tumor effects through ROS generation and lipid peroxidation, leading to multi-modal cell death responses. This mechanistic overlap raises the possibility that combined administration of temsirolimus and 5-FU may shift cell death pathways towards ferroptosis, potentially superseding pyroptosis. Additionally, recent studies demonstrate that caspase-3 can cleave GSDME, resulting in membrane pore formation and pyroptotic cell lysis in cells with high GSDME expression [30, 31]. In contrast, cells with low GSDME levels primarily undergo apoptosis following caspase-3 activation. This bimodal regulatory mechanism suggests that GSDME-mediated pyroptosis is highly context-dependent and may not serve as the principal cytotoxic pathway in malignancies with low GSDME expression. Given the evolving understanding of pyroptosis in initiating anti-tumor immune responses, therapeutic strategies modulating this pathway could significantly influence immunotherapeutic outcomes. Therefore, it is critical to investigate whether ferroptosis can functionally compensate for pyroptosis within the context of synergistic regimens combining mTOR pathway inhibitors and cell cycle-targeting agents.

Materials and methods

Clinical samples

A total of 16 high-grade serous epithelial ovarian cancer (HGSC) tissue samples and their paired adjacent normal tissues were collected from patients at the Chinese PLA General Hospital. All specimens were immediately frozen at -80°C for subsequent analyses. The study protocol was approved by the Ethics Committee of the Chinese PLA General Hospital, and all procedures involving human participants were conducted in accordance with the Helsinki Declaration. Written informed consent was obtained from each participant prior to surgical tissue collection.

Cell culture and reagents

The human ovarian cancer cell lines A2780 and OVCAR3 were obtained from the Cell Bank of the Chinese Academy of Sciences (Shanghai, China). Cells were routinely cultured in DMEM (Gibco, Carlsbad, CA, USA) supplemented with 10% fetal bovine serum (FBS) and maintained at 37°C in a humidified incubator with 5% CO_2. Media were refreshed every 1-2 days, and cells were passaged into new 6 cm dishes upon reaching > 90% confluence. To determine whether GSDMD or GSDME mediates chemotherapy-induced pyroptosis in ovarian cancer cells, A2780 and OVCAR3 cell lines were exposed for 48 h to various chemotherapeutic agents: 5-FU (100 mM), temsirolimus (50 μM), a combination of 5-FU (100 mM) and temsirolimus (50 μM), cisplatin (5 mg/mL), pemetrexed (10 mmol/L), paclitaxel (50 nM), and doxorubicin (400 ng/mL).

Microscopy imaging

To evaluate pyroptotic morphology, cells were seeded in 6-well culture plates and subjected to indicated treatments. Brightfield and fluorescence images were captured using an Olympus IX73 fluorescence microscope at magnifications of 100× and 200×.

Hoechst/propidium iodide nuclear staining

To evaluate cell death morphology, A2780 and OVCAR3 cells were treated with 5-FU alone or in combination with temsirolimus for 48 h and imaged using fluorescence microscopy. Apoptotic and necrotic cells were identified using the Apoptosis and Necrosis Assay Kit (Beyotime Institute of Biotechnology) following the manufacturer's protocol. Briefly, cells were incubated with 10 ng/mL Hoechst 33342 and 10 ng/mL propidium iodide (PI) for 20 min at 0°C in the dark. The cells were then quantified using an Olympus fluorescence microscope.

Western blotting

Tumor tissues excised during surgery were stored at -80°C. For protein extraction, 100-200 mg (wet weight) of frozen tissue was minced with a scalpel blade and homogenized

in 15 mL of ice-cold RIPA (Radioimmunoprecipitation Assay) lysis buffer containing 1% protease inhibitor cocktail (Sigma, St. Louis, MO, USA). Cancer cell lines were similarly lysed using RIPA buffer supplemented with 1% protease inhibitors. Tissue and cell lysates were centrifuged at 12,000 rpm for 5 min at 4°C, and total protein concentrations were determined using a bicinchoninic acid (BCA) Protein Assay Kit (Pierce, Rockford, IL, USA). Equal amounts of protein were separated by electrophoresis on a 10% SDS-PAGE gel (Bio-Rad, Hercules, CA, USA) and subsequently transferred onto polyvinylidene difluoride (PVDF) membranes (Millipore, Billerica, MA, USA). Membranes were blocked with 5% non-fat milk for 1 h at room temperature, followed by overnight incubation at 4°C with primary antibodies: GSDMD and GSDMD N-terminal (Abcam, Cambridge, UK), GSDME and GSDME N-terminal (Abcam), Poly (ADP-ribose) Polymerase-1 (PARP-1) and cleaved PARP-1 (Santa Cruz Biotechnology, Dallas, TX, USA), β-actin (Santa Cruz Biotechnology), GPX4 (Abcam), and ACSL4 (Abcam). After washing, membranes were incubated with horseradish peroxidase (HRP)-conjugated goat anti-rabbit or anti-mouse IgG secondary antibodies (Santa Cruz Biotechnology) for 2 h at room temperature. Protein bands were visualized using enhanced chemiluminescence (ECL) detection (Millipore) and analyzed with a Tanon 1600 imaging system (Tanon, Shanghai, China).

siRNA experiments

To investigate the role of GSDME in chemotherapy-induced pyroptosis in ovarian cancer cells, small interfering RNA (siRNA) targeting human GSDME, along with a corresponding negative control siRNA, were obtained from GeneChem (Shanghai, China). The siRNA sequences of negative control and GSDME were as follows:

Negative control: 5'-UUCUCCGAACGUGUCACGUTT-3',

GSDME siRNA (1): 5'-GCAGCAAGCAGCUGUUUAUTT-3',

GSDME siRNA (2): 5'-GAGAGGAATTTCCATCCATTT-3'.

To elucidate the mechanisms underlying GSDME cleavage and activation, specifically the roles of caspase-3 and caspase-7, OVCAR3 cells were transfected with siRNAs targeting human caspase-3 (sc-29237) and caspase-7 (sc-29929) as well as a negative control siRNA. All siRNAs were purchased from Santa Cruz Biotechnology (Shanghai, China). A2780 and OVCAR3 cells were seeded at a density of 2×10^5 cells/mL and transfected with either GSDME-specific siRNA or negative control siRNA using Lipofectamine 3000, following the manufacturer's instructions. The transfection medium was replaced with fresh complete medium supplemented with 10% fetal bovine serum (FBS) at 24 h post-transfection. Cells were incubated for an additional 24-48 h prior to collection for subsequent analyses.

Cell viability assay

Cell viability was quantified using the Cell Counting Kit-8 (CCK-8; Lianke Bio, Hangzhou, China). Treated cells were seeded in 96-well plates at a density of 5×10^3 cells per well in 100 μL of culture medium. At 48 h, 10 μL of CCK-8 reagent was added to each well, followed by incubation for 4 h at 37°C. Absorbance at 450 nm was measured using a microplate reader (Biotek, Winooski, VT, USA) to determine cell viability. A 10-point dose-response curve was generated in the CCK-8 assay for both 5-FU (0.1 μM to 100 mM) and temsirolimus (0.01 μM to 200 μM). All dose-response data were analyzed using a nonlinear regression model with a four-parameter logistic function, as implemented in GraphPad Prism software (version 9.3.1). The concentration points of 5-FU and temsirolimus employed in subsequent experiments to evaluate GSDME and its N-terminal fragment expression were determined based on inflection points identified in the fitted viability curves.

Measurement of malondialdehyde

Malondialdehyde (MDA) concentrations were quantified using a commercial ELISA kit (Elabscience, Wuhan, China) according to the manufacturer's protocol. Briefly, 50 μL of standard, blank, and sample were dispensed into individual wells of a 96-well plate, followed by the addition of 50 μL biotinylated detection antibody working solution. Plates were incubated for 45 minutes at 37°C. After washing, 100 μL HRP conjugate working solution was added, and plates were incubated for an additional 30 minutes at 37°C. Following wash, 90 μL substrate reagent was added to each well and incubated for 15 minutes at 37°C in the dark. Finally, 50 μL stop solution was added, and absorbance was measured at 450 nm using a microplate reader.

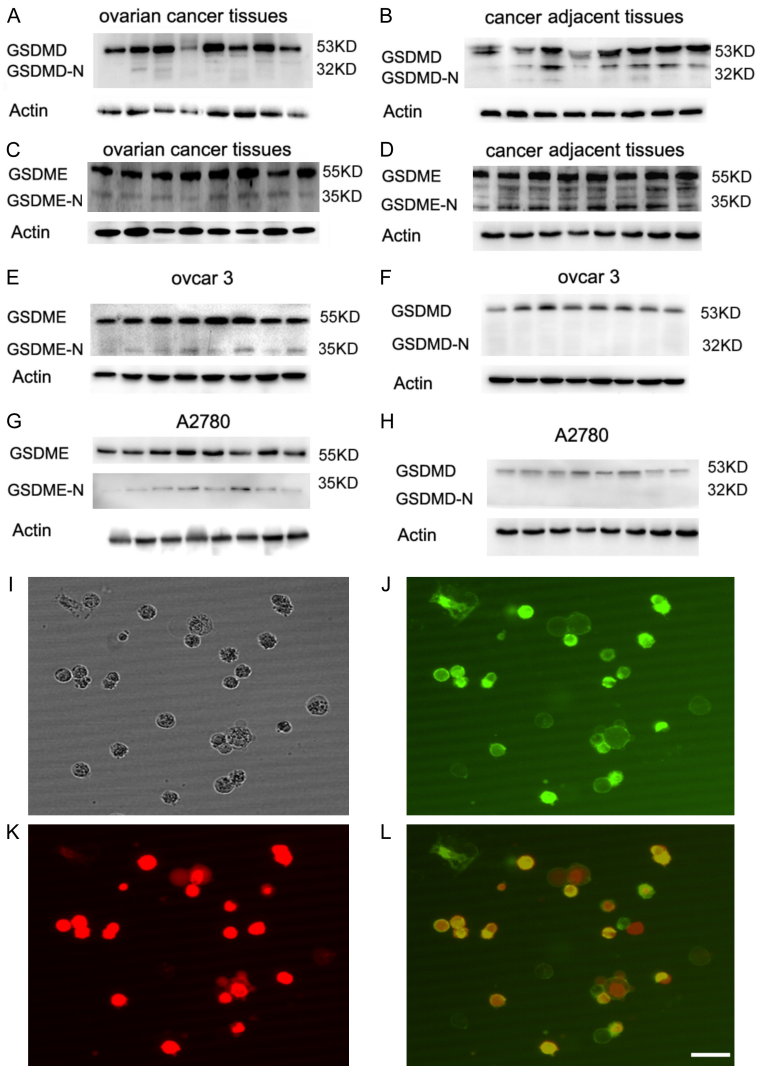

Figure 1. Expression of GSDMD, GSDME, and their N-terminal fragments in ovarian cancer tissues and cell lines. (A, B) Full-length GSDMD was detected in both ovarian cancer and adjacent non-cancerous tissues, whereas the GSDMD N-terminal fragment is detectable only in cancer tissues. (C, D) Both full-length GSDME and its N-terminal fragment were present in ovarian cancer tissues; the GSDME N-terminal fragment was absent in adjacent non-cancerous tissues. (E-H) In OVCAR3 and A2780 cell lines, both full-length GSDMD and GSDME were present, but after treatment with chemotherapeutic agents (DMSO, 5-FU [100 mM], temsirolimus [50 μM], 5-FU + temsirolimus, cisplatin [5 mg/mL], pemetrexed [10 mmol/L], paclitaxel [50 nM], doxorubicin [400 ng/mL]), only the GSDME N-terminal fragment was detected. GSDME and its N-terminal in OVCAR3 cells (E); GSDMD and its N-terminal in OVCAR3 cells (F); GSDME and its N-terminal in A2780 cells (G); GSDMD and its N-terminal in A2780 cells (H). (I-L) In 5-FU-treated OVCAR3 cells, bubble-like pyroptotic morphology and double Annexin V/PI staining confirm the induction of pyroptosis. Scale bar = 50 μm, 200×.

Statistical analysis

All experimental assays were independently performed at least three times, with each experiment comprising three technical replicates. Prior to applying parametric statistical tests, the normality of data distributions was assessed using the Shapiro-Wilk test, while homogeneity of variance was evaluated with Levene's test. For comparisons between two groups, Student's t-test was employed when both normality and variance homogeneity criteria were met; otherwise, the non-parametric Mann-Whitney U test was utilized. For analyses involving more than two groups, one-way analysis of variance (ANOVA) was conducted following verification of parametric assumptions. Post-hoc comparisons were performed using Tukey's test, or Dunnett's test when comparing multiple groups against a single control. If parametric assumptions were violated, the non-parametric Kruskal-Wallis test was applied, followed by Dunn's post-hoc test. Statistical analyses, including t-tests, ANOVA, non-parametric tests, and post-hoc procedures, were executed using GraphPad Prism version 9.3.1, while Microsoft Excel 2016 was utilized for data organization and preliminary descriptive statistics. Statistical significance was defined as $P < 0.05$.

Results

Expression of GSDMD and GSDME proteins in human ovarian cancer tissues, adjacent normal tissues, and cell lines

To investigate the involvement of pyroptosis in ovarian cancer, the expression profiles of pyroptosis-associated proteins GSDMD and GSDME were evaluated in ovarian cancer tissues and matched adjacent non-cancerous tissues using Western blot analysis. Representative electropherograms from 16 patients are presented in **Figure 1A**, **1B** and Supplementary Figure 1A, 1B. GSDMD protein

was detected in both cancerous and adjacent non-cancerous tissues; however, the cleaved N-terminal fragment of GSDMD (GSDMD-N) was exclusive to cancerous tissues. In contrast, both full-length and N-terminal fragments of GSDME were identified in ovarian cancer and adjacent normal tissues (**Figure 1C**, **1D** and Supplementary Figure 1C, 1D). These findings suggest that, even in treatment-naïve ovarian cancer patients, pyroptosis predominantly occurs via GSDME cleavage.

Next, GSDMD and GSDME expressions were assessed in ovarian cancer cell lines OVCAR3 and A2780. Both cell lines expressed detectable levels of full-length GSDMD and GSDME. To determine the capacity of various chemotherapeutic agents to induce pyroptosis and to identify the responsible gasdermin family member, cells were treated with 5-FU (100 mM), temsirolimus (50 μM), a combination of temsirolimus and 5-FU, cisplatin (5 mg/mL), pemetrexed (10 mmol/L), paclitaxel (50 nM), or doxorubicin (400 ng/mL) for 48 h. Notably, only the cleaved N-terminal fragment of GSDME (GSDME-N) was detected following treatment, whereas GSDMD-N remained undetectable (**Figure 1E-H** and Supplementary Figure 1E, 1F).

To elucidate the mechanisms underlying GSDME activation, OVCAR3 cells were transfected with siRNAs targeting caspase-3 and caspase-7 (Santa Cruz Biotechnology). Western blot confirmed efficient knockdown of caspase-3 and caspase-7 protein expression 48 h post-transfection (caspase-3: 81 ± 6% reduction; caspase-7: 78 ± 4% reduction relative to control siRNA, Supplementary Figure 1G, 1H). Cells were subsequently treated with 5-FU and temsirolimus, and caspase knockdown markedly diminished the formation of the GSDME N-terminal fragment compared to control siRNA and drug-treated cells (Supplementary Figure 1I, 1J). These results indicate that both caspase-3 and caspase-7 are required for generating the active GSDME N-terminal fragment under these conditions.

Pyroptotic cells were identified by combining morphological criteria (membrane blebbing) with Annexin V/PI staining. OVCAR3 cells treated with chemotherapeutic agents exhibited membrane blebbing, a hallmark of pyroptosis (**Figure 1I**). Annexin V^+/PI^+ staining was used to differentiate early apoptotic (Annexin V^+/PI^-) and late apoptotic or pyroptotic cells (Annexin V^+/PI^+), as previously established [32]. All cells displaying membrane blebbing were also Annexin V^+/PI^+, confirming the association of these markers with pyroptotic morphology (**Figure 1I-L**). Pyroptotic cells accounted for 15-20% of the total Annexin V^+/PI^+ population.

Collectively, although GSDMD and GSDME proteins are present in both tumor and adjacent normal tissues of chemotherapy-naïve ovarian cancer patients, only the cleaved N-terminal fragment of GSDME was prominent in cancerous tissues (**Figure 1A-D**). This finding suggests that pyroptosis potential exists in both tissue types, but GSDME cleavage is preferentially activated in tumor tissues, providing a rationale for further investigation of GSDME-mediated pyroptosis in ovarian cancer progression. Similarly, OVCAR3 and A2780 cell lines expressed full-length GSDMD and GSDME, yet only the cleaved N-terminal fragment of GSDME was observed after chemotherapy treatment (**Figure 1E-H**), indicating that chemotherapy-induced pyroptosis in ovarian cancer cells is primarily mediated by GSDME activation.

GSDME, but not GSDMD, mediates differential levels of pyroptosis in ovarian cancer cells following temsirolimus and 5-FU treatment

To elucidate the molecular mechanisms underlying the synergistic cytotoxicity of 5-FU and temsirolimus in ovarian cancer cells, cell viability and cell death pathways were assessed following monotherapy with each agent. CCK-8 assays showed that both temsirolimus and 5-FU dose-dependently reduced the viability of OVCAR3 and A2780 cells. Temsirolimus significantly decreased cell viability at concentrations between 20 and 100 μM (IC_{50}: 24.7 μM for OVCAR3, 25.8 μM for A2780), whereas 5-FU induced notable viability reduction at 200 μM and maximal effect at 100 mM (IC_{50}: 354.5 mM for OVCAR3, 289.8 mM for A2780). These concentrations were selected for subsequent experiments (**Figure 2A**, **2B**).

Western blot revealed dose-dependent GSDME cleavage in temsirolimus-treated cells, and to a lesser extent with 5-FU, indicating differential activation of GSDME-mediated pyroptosis (**Figure 2C**, **2E**). Temsirolimus, but not 5-FU, also induced dose-dependent cleavage of PARP-1,

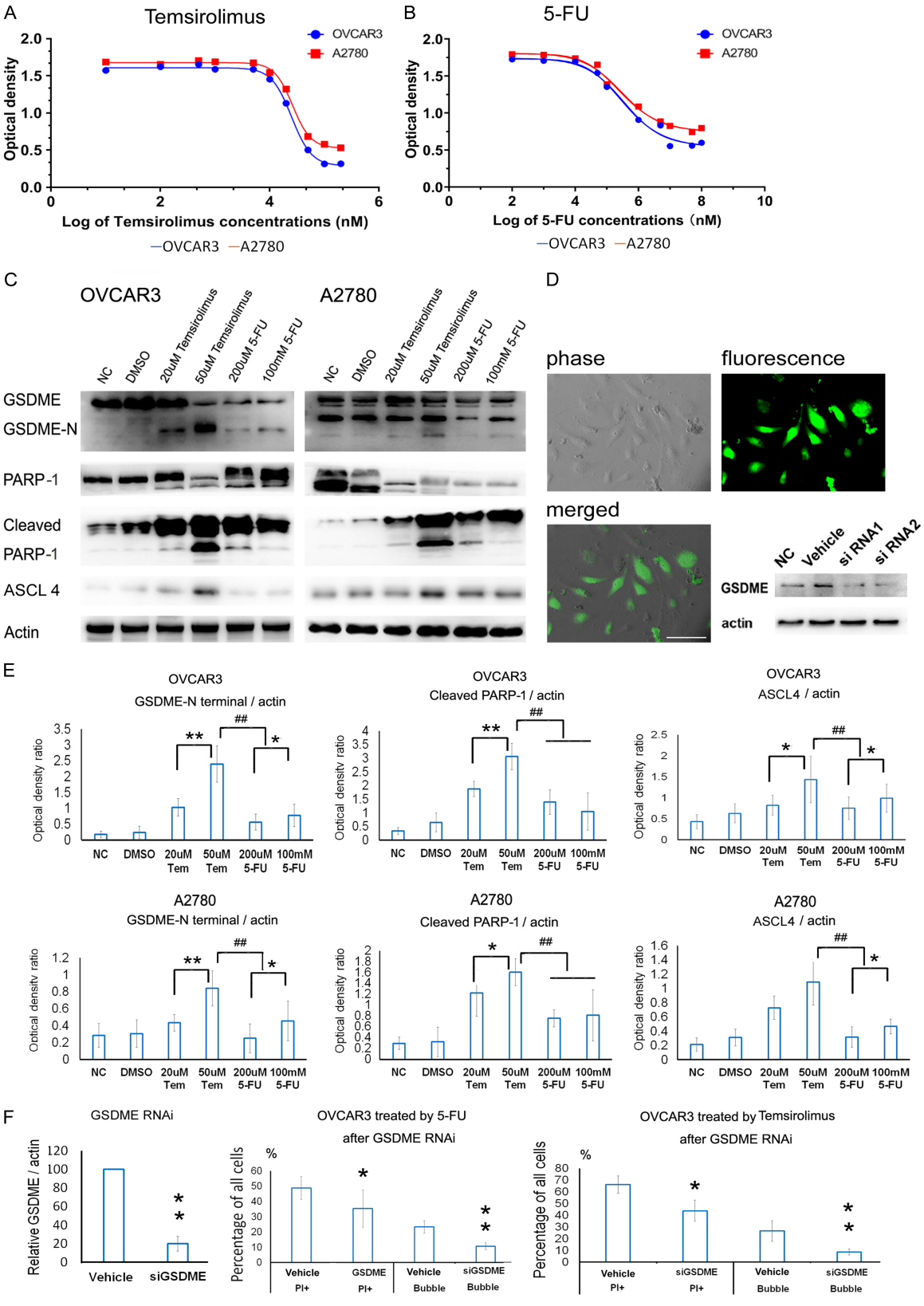

Figure 2. Temsirolimus and 5-FU induce pyroptosis to varying extents via GSDME activation. A, B. CCK-8 assay demonstrated dose-dependent inhibition of cell viability by 5-FU and temsirolimus in both OVCAR3 and A2780 cell lines. C. Western blot analysis of GSDME, cleaved GSDME-N, PARP-1, cleaved PARP-1, and ACSL4 in OVCAR3 and A2780 cells following treatment with temsirolimus (20 μM, 50 μM) and 5-FU (200 μM, 100 mM). D. GSDME siRNA

transfection achieved ~90% efficiency and markedly reduced GSDME protein expression in OVCAR3 cells. E. Quantitative analysis indicated dose-dependent increases in GSDME-N, cleaved PARP-1, and ACSL4 with temsirolimus and 5-FU treatments in both cell lines. The effects of temsirolimus were significantly greater than those of 5-FU for GSDME cleavage, PARP-1 cleavage, and ACSL4 upregulation (n = 4; *P < 0.05, **P < 0.01 vs. lower concentration; #P < 0.05, ##P < 0.01 vs. 50 μM temsirolimus vs. 5-FU). F. GSDME knockdown in OVCAR3 cells reduced GSDME expression to 20-30% of control and decreased the percentage of PI-positive and pyroptotic cells following 5-FU or temsirolimus treatment (n = 4; *P < 0.05, **P < 0.01 vs. vehicle siRNA). Scale bar = 50 μm, 200×.

signifying greater apoptotic activation (**Figure 2C**, **2E**). Both agents modulated the ferroptosis marker ACSL4, though 5-FU had a significantly weaker effect compared to temsirolimus.

The formation of the GSDME-N fragment (35 kDa) in both cell lines supports GSDME-mediated pyroptosis as a primary cell death pathway. Knockdown of GSDME in OVCAR3 cells via siRNA (> 90% transfection efficiency, ~80% knockdown) markedly decreased temsirolimus- and 5-FU-induced cell death, as shown by reduced PI staining and lower proportions of pyroptotic cells (**Figure 2D**, **2F**). Collectively, these findings demonstrate that GSDME plays a central role in chemotherapy-induced pyroptosis and cytotoxicity in ovarian cancer cells.

GSDME-dependent pyroptosis is critical for the synergistic cytotoxic effects of combined temsirolimus and 5-FU treatment

Synergistic anti-proliferative effects of temsirolimus (mTOR inhibitor) combined with 5-FU were evaluated in A2780 and OVCAR3 cells using CCK-8 assays after 48 h treatment. Immunoblot analysis of phosphorylated S6 (p-S6), a downstream mTOR target, confirmed mTOR pathway inhibition by temsirolimus alone and in combination with 5-FU (**Figure 3A**). Combined treatment produced greater reduction in cell viability than either drug alone; maximal suppression in both cell lines was achieved with 100 μM 5-FU and 5 μM temsirolimus (**Figure 3B**), concentrations used for subsequent experiments. Microscopy revealed prominent pyroptotic morphology, with bubble-like membrane rupture in most combination-treated cells (**Figure 3C**). Western blot showed significantly increased cleaved GSDME-N fragment (35 kDa) with combination therapy versus monotherapy (**Figure 3D**, **3E**). GSDME silencing via siRNA attenuated the cytotoxic effect of combination therapy, with cell viability decreasing to 40-50% in knockdown cells compared to 20-30% in wild-type controls (**Figure 3F**, **3G**). These findings indicate that GSDME-mediated pyroptosis is essential for the enhanced anti-tumor effects of combined temsirolimus and 5-FU in ovarian cancer cells.

Oxidative stress mediates the concomitant induction of multiple cell death pathways by temsirolimus and 5-FU

Chemotherapy can induce multiple cell death pathways in cancer cells. To assess the involvement of apoptosis and ferroptosis in the combined action of temsirolimus and 5-FU in ovarian cancer cells, we analyzed pathway-specific protein markers using Western blotting. Combination treatment significantly increased cleaved PARP-1, indicating enhanced apoptosis, while concurrently reducing GPX4 levels, consistent with induction of ferroptosis, in both OVCAR3 and A2780 cells (**Figure 4A**, **4B**). These results suggest that temsirolimus and 5-FU together activate multiple cell death mechanisms - including pyroptosis, apoptosis, and ferroptosis - likely through oxidative stress mediated by reactive oxygen species and lipid peroxidation.

ROS, generated as byproducts of cellular oxygen metabolism, play a regulatory role in apoptosis and autophagy [27] and serve as potent inducers of ferroptosis in various pathological contexts [29]. Accumulated ROS promote lipid peroxidation, a key indicator of oxidative damage, and can also activate inflammasome-dependent pyroptosis [33]. However, the extent to which temsirolimus- or 5-FU-induced oxidative stress mediates pyroptosis, apoptosis, or ferroptosis in ovarian cancer cells remains to be fully elucidated.

To evaluate the role of ROS in mediating the synergistic cytotoxicity of temsirolimus and 5-FU, N-acetyl-L-cysteine (NAC) was utilized as a ROS scavenger and lipid peroxidation inhibitor. NAC functions as a precursor for glutathione (GSH) synthesis, thereby neutralizing ROS and mitigating mitochondrial lipid peroxidation. Previous studies have shown that ferroptosis

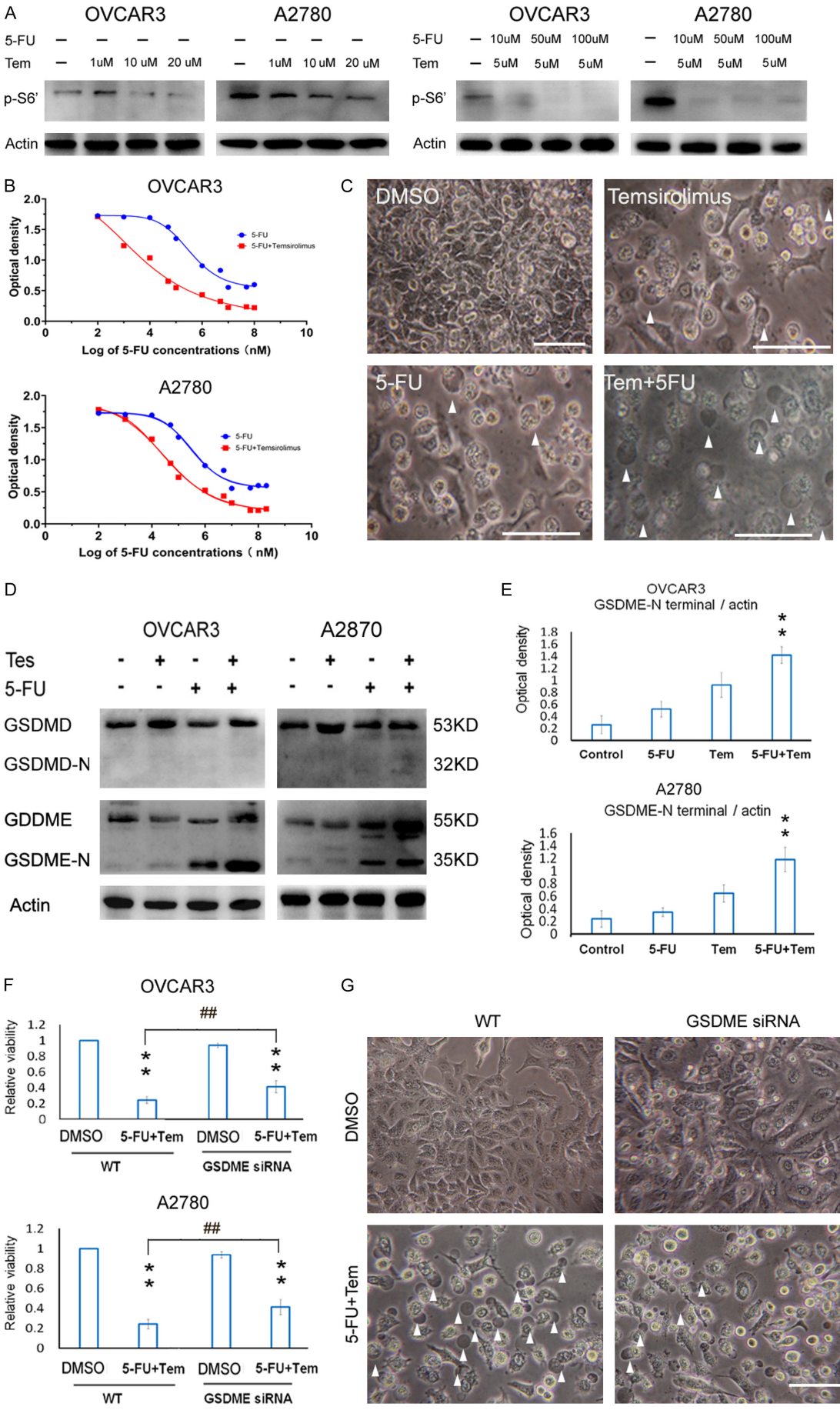
A
OVCAR3
A2780
OVCAR3
A2780
5-FU
Tem
1uM 10 uM 20 uM
10uM 50uM 100uM
5uM 5uM 5uM
p-S6'
Actin
B
OVCAR3
Optical density
5-FU
5-FU+Temsirolimus
Log of 5-FU concentrations (nM)
A2780
C
DMSO
Temsirolimus
5-FU
Tem+5FU
D
OVCAR3
A2870
Tes
5-FU
GSDMD
GSDMD-N
GDDME
GSDME-N
Actin
53KD
32KD
55KD
35KD
E
OVCAR3
GSDME-N terminal / actin
Optical density
Control
5-FU
Tem
5-FU+Tem
A2780
GSDME-N terminal / actin
F
OVCAR3
Relative viability
##
DMSO
5-FU+Tem
WT
GSDME siRNA
A2780
G
WT
GSDME siRNA
DMSO
5-FU+Tem

Figure 3. Temsirolimus and 5-FU combination induces GSDME-dependent pyroptosis. A. Phosphorylation of ribosomal protein S6 (rpS6), a downstream mTOR effector, was assessed using anti-p-S6 (Ser235/236) antibody. Temsirolimus induced significant downregulation of p-rpS6. The combination with 5-FU synergistically blocked mTOR activation and downstream signaling. B. CCK-8 assays demonstrated enhanced synergistic anticancer effects in ovarian cancer cell lines compared to 5-FU or temsirolimus monotherapy. C. OVCAR-3 cellular morphology demonstrated characteristic pyroptotic features with membrane-blebbing vesicles under combination therapy, showing enhanced pyroptosis induction compared to 5-FU or temsirolimus monotherapy. Scale bar = 50 μm, 100× in DMSO while 200× in temisirolimus, 5-FU, and Tem + 5-FU. D, E. The expression of GSDME-N terminal in A2780 and OVCAR3 cells was significantly increased by combination therapy as compared to the single use of them. The GSDMD N-terminal was not clearly observed with the combined treatment. **P < 0.01, compared to 5-FU or temsirolimus respectively. F. GSDME knockout abrogated the therapeutic efficacy of temsirolimus/5-FU combination, achieving 40-50% tumor growth of DMSO group, versus 20-30% in wild-type siRNA control group. P < 0.01, compared to DMSO group. P < 0.01, siRNA vs. wide type control. G. After GSDME RNAi, the representative morphology of OVCAR3 under the combined treatment of 5-FU and temsirolimus. The GSDME RNAi significantly decreased the ratio of typical bubble-like cells when treated by the combination therapy. **P < 0.01, compared to DMSO group. N = 5. Scale bar = 50 μm, ×200, Tem: Temsirolimus.

agonists, such as erastin and Ras-selective lethal 3 (RSL3), enhance ROS generation and lipid peroxidation when combined with temsirolimus [29]. Quantification of malondialdehyde (MDA), a marker of lipid peroxidation, demonstrated that both temsirolimus/5-FU and temsirolimus/RSL3 treatments significantly elevated MDA levels in OVCAR3 and A2780 cells, with the RSL3 combination producing a more pronounced increase compared to 5-FU (**Figure 4C**). Cell viability assays revealed that NAC reversed the cytotoxic effects of temsirolimus combined with either 5-FU or RSL3 in both cell lines (**Figure 4D**). Additionally, NAC treatment substantially reduced the expression of cleaved PARP-1 (apoptosis marker) and the GSDME-N terminal fragment (pyroptosis marker) in cells exposed to temsirolimus/5-FU or temsirolimus/RSL3 (**Figure 4E-H**). Western blot analysis further showed that NAC significantly restored GPX4 expression compared to temsirolimus/5-FU or temsirolimus/RSL3 treatments (**Figure 4E-H**). These findings suggest that RSL3 potentiates temsirolimus-induced ferroptosis more effectively than 5-FU, and that ROS plays a central role in mediating the combination-induced cell death pathways.

Discussion

Previous studies have demonstrated that expression levels of pyroptosis markers correlate with pathological grading in various cancers; for example, caspase-1, GSDMD, and IL-1β have been associated with proliferation, invasion, and metastasis in breast cancer [34]. In ovarian cancer, most research to date has focused on GSDMD [16-19]. In this study, we explored the role of GSDME, a major pyroptosis effector, in ovarian carcinoma tissues and cell lines. Analysis of 16 chemotherapy-naïve ovarian cancer tissue samples and matched adjacent normal tissues revealed detectable levels of GSDMD and GSDME in both types of tissues. Notably, only the cleaved N-terminal fragment of GSDME was present exclusively in tumor tissues. These observations suggest that GSDME may play a critical role in ovarian cancer progression [16-19].

Following chemotherapeutic treatment, both GSDME and its cleaved N-terminal fragment were detected in ovarian cancer cell lines (OVCAR3 and A2780), whereas the active N-terminal fragment of GSDMD remained undetectable even at higher drug concentrations (**Figure 2C**). Pyroptosis was confirmed by increased PI/Annexin V double staining and the presence of membrane blebbing, a morphological hallmark of pyroptosis. Temsirolimus and 5-FU significantly reduced cell viability and increased the proportion of PI/Annexin V double-positive cells with pyroptotic features compared to controls. Both agents upregulated GSDME-N terminal expression and activated apoptotic and ferroptotic pathways, with temsirolimus eliciting stronger pyroptotic and apoptotic effects than 5-FU. siRNA-mediated knockdown of GSDME substantially decreased the number of pyroptotic cells and reduced the overall contribution of pyroptosis to cell death (**Figure 2C**). These findings indicate that GSDME-mediated pyroptosis is a principal cell death pathway in ovarian cancer cells treated with temsirolimus or 5-FU. Additionally, our data demonstrate that both caspase-3 and caspase-7 are required for GSDME cleavage in OVCAR3 cells following chemotherapy, consistent with recent reports implicating multiple caspases in GSDME activation [3, 30].

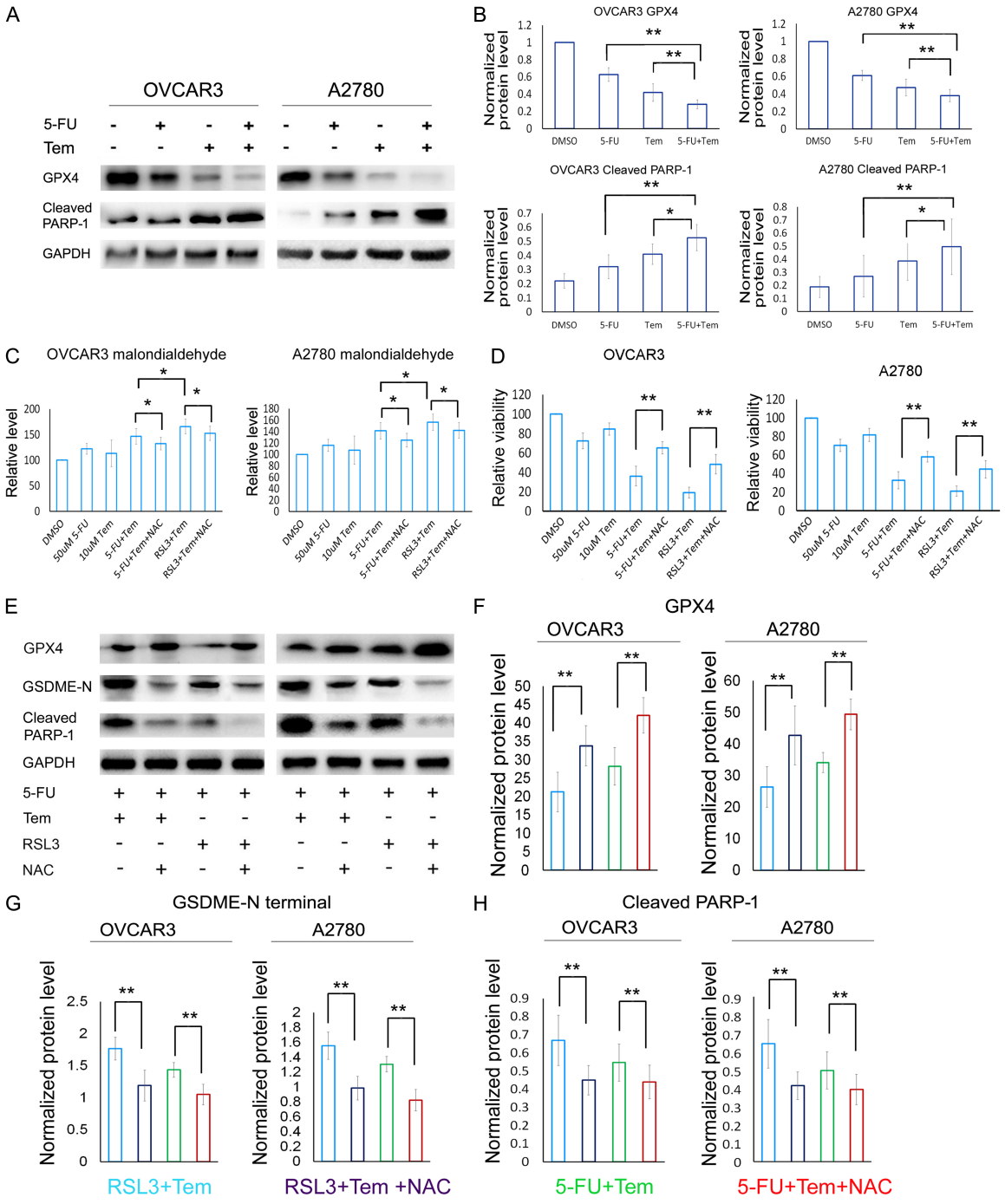

Figure 4. NAC reverses the synergistic increase in MDA and cytotoxicity induced by temsirolimus combined with 5-FU or RSL3 in ovarian cancer cells. A, B. Temsirolimus/5-FU combination significantly suppressed PARP-1 and GPX4 protein expression in OVCAR-3 and A2780 cells versus monotherapies (*P < 0.05). C. Co-treatment with temsirolimus plus RSL3/5-FU elevated MDA levels in both cell lines, with RSL3 combinations inducing 2.3-fold higher MDA than 5-FU regimens (**P < 0.01). D. NAC restored cell viability in RSL3/temsirolimus and 5-FU/temsirolimus treated groups (**P < 0.01). E-H. In the synergistic treatment of “5-FU + temsirolimus” and “RSL3 + temsirolimus”, the addition of NAC significantly reversed the expression of apoptosis specific protein, PARP-1, ferroptosis specific protein GPX4, and pyroptosis execution protein GSDME N-terminal. Scale bar = 50 μm, 200×.

The therapeutic strategy of combining PI3K-AKT-mTOR inhibitors with traditional cell cycle inhibitors has been investigated in previous studies. For instance, Wagner et al. demon-

strated that rapamycin combined with 5-FU or oxaliplatin resulted in enhanced antitumor efficacy relative to rapamycin monotherapy [35]. Similarly, Kollmannsberger et al. reported the safe co-administration of temsirolimus with carboplatin and paclitaxel in patients with advanced solid tumors [11]. More recently, the use of ferroptosis inducers alongside cisplatin has been explored for ovarian cancer treatment [25]. Despite these advances, the distinct cell death pathways engaged by combination chemotherapies remain inadequately characterized. Although pyroptosis has been recognized as a contributor to cancer cell death [36], its specific role in ovarian cancer, especially in the context of monotherapy versus combination therapy, requires further elucidation [37].

The PI3K-AKT-mTOR pathway is integral to cancer cell metabolism and redox homeostasis, with inhibition leading to increased ROS accumulation and lipid peroxidation, key mechanisms underlying ferroptosis. Recent studies have shown that combining temsirolimus, an mTOR inhibitor, with RSL3, a ferroptosis inducer and GPX4 inhibitor, synergistically augments oxidative stress, driving potent ferroptosis and achieving near-complete tumor regression in preclinical models [29]. To expand upon these findings, we examined whether the combination of temsirolimus with 5-FU, a DNA replication inhibitor, activates multiple cell death pathways in ovarian cancer cells. Our results demonstrate that dual treatment with temsirolimus and 5-FU produces substantially greater tumor growth inhibition than either agent alone, with simultaneous activation of pyroptosis, apoptosis, and ferroptosis. Importantly, siRNA-mediated knockdown of GSDME attenuated pyroptosis and therapeutic efficacy, establishing GSDME-dependent pyroptosis as essential for the cytotoxic effects of this regimen. These findings support emerging evidence that chemotherapy-induced cell death in ovarian cancer involves a coordinated interplay of ferroptosis, pyroptosis, and apoptosis [25].

ROS are well-known inducers of apoptosis and are implicated in various pathological processes [27]. Additionally, ROS can activate inflammasome-dependent pyroptosis in parallel with apoptosis [33]. To evaluate oxidative stress, malondialdehyde (MDA), a terminal lipid peroxidation product, was measured in treated cells. Results indicated that lipid peroxide accumulation directly mediates the simultaneous activation of pyroptosis, apoptosis, and ferroptosis. Comparison of tumor-suppressive efficacy between temsirolimus combined with either the ferroptosis inducer RSL3 or the DNA replication inhibitor 5-FU revealed significantly greater inhibition of ovarian cancer cell growth with the RSL3 + temsirolimus regimen [29]. This combination also led to markedly higher MDA levels than the temsirolimus plus 5-FU treatment, indicating enhanced lipid peroxidation. Moreover, treatment with N-acetyl-L-cysteine (NAC), a ferroptosis inhibitor acting through mitochondrial pathways, reversed the cytotoxicity of both drug combinations in ovarian cancer cells. These findings demonstrate that ROS are central mediators of cell death mechanisms induced by these therapeutic strategies.

Crosstalk exists between GSDME and oxidative stress. Combined temsirolimus and 5-FU treatment synergistically increases intracellular ROS, leading to caspase-3 activation. ROS-mediated calcium influx further amplifies caspase-3 signaling, establishing a positive feedback loop that intensifies apoptotic cascades. Activated caspase-3 cleaves full-length GSDME into its N-terminal pore-forming fragment, which oligomerizes on the plasma membrane to induce pyroptosis. Functional studies revealed that siRNA-mediated GSDME knockdown significantly reduces the generation of the pyroptotic N-terminal fragment after combination treatment, mechanistically linking ROS to GSDME-dependent pyroptotic cell death (**Figure 4**). In addition, a theoretical feedback loop may exist between oxidative stress and GSDME-mediated pyroptosis. Pyroptotic cells release damage-associated molecular patterns (DAMPs), such as ATP and high-mobility group box 1 (HMGB1), which activate purinergic receptors and TLR4 signaling in neighboring cells. This activation intensifies oxidative stress through NADPH oxidase stimulation and mitochondrial dysfunction, potentially establishing a self-amplifying cycle that enhances antitumor efficacy.

Cancer cells harboring PI3K-AKT-mTOR pathway mutations often reprogram lipid metabolism, conferring resistance to ferroptosis. Dual inhibition by temsirolimus (targeting mTOR) and RSL3 (a GPX4 inhibitor) exerts potent antitumor effects by inducing ferroptosis and leading to regression of multiple solid tumors [29].

This demonstrates the synergistic efficacy of combined mTOR and GPX4 inhibition. Traditional chemotherapeutics such as high-dose 5-FU also induce ROS, mimicking oxidative stress associated with GPX4 inhibition. Based on this mechanistic overlap, we hypothesized that combinations of PI3K-AKT-mTOR inhibitors and cell cycle inhibitors could replicate the therapeutic benefits seen with dual GPX4/mTOR inhibitors. However, our data show that even at high concentrations, cell cycle inhibitors combined with mTOR inhibitors do not fully shift cell death from pyroptosis to ferroptosis. Mechanistic studies confirmed that this drug combination activates multiple cell death pathways - including pyroptosis, apoptosis, and ferroptosis - within ovarian cancer cells. These findings establish pyroptosis as an indispensable contributor to the therapeutic efficacy of chemotherapy regimens including PI3K-AKT-mTOR inhibitors and cell cycle inhibitors, either as monotherapy or in combination.

This study has several limitations. First, the concentrations of 5-FU and temsirolimus used in vitro exceed clinically achievable plasma levels, which may lead to an overestimation of oxidative stress-mediated pyroptosis. Further investigations using prolonged exposure to clinically relevant drug concentrations are necessary to evaluate the kinetics of GSDME-dependent pyroptosis under physiological conditions. Second, differences in drug response between the OVCAR3 and A2780 cell lines were observed. These cell lines possess distinct genetic backgrounds, mutation profiles, and baseline sensitivities to chemotherapeutic agents, impacting their resistance mechanisms - including enhanced DNA repair, altered drug accumulation, increased efflux, chromosomal instability, and stemness-associated traits. Consequently, they exhibit differential patterns of chemoresistance under the experimental conditions employed. Third, while our data mechanistically implicate pyroptosis as a synergistic cell death pathway following 5-FU and temsirolimus treatment, in vivo validation remains essential. Future studies employing pyroptosis-deficient tumor models, such as GSDME-knockout xenografts, will be necessary to confirm the translational relevance of pyroptosis induction in the therapeutic context.

In conclusion, this study provides direct evidence of GSDME-mediated pyroptosis in ovarian cancer tissues. Neither 5-FU nor temsirolimus, alone or in combination, is capable of fully shifting pyroptosis to ferroptosis. Pyroptosis is a critical cytotoxic mechanism in chemotherapy regimens targeting the cell cycle or PI3K-AKT-mTOR pathway, operating through ROS-dependent processes in both monotherapy and combination settings. Notably, targeting pyroptosis may offer a therapeutic avenue to overcome apoptosis resistance in cancer treatments [4, 5]. Moreover, emerging evidence implicates pyroptosis in the activation of antitumor immunity [15], indicating that strategic modulation of oxidative stress-induced pyroptosis and its immunogenic consequences could improve chemotherapy efficacy. Further studies into these pathways may reveal novel approaches for the treatment of ovarian cancer.

Disclosure of conflict of interest

None.

Address correspondence to: Yuanguang Meng, Department of Gynecology and Obstetrics, People's Liberation Army (PLA) Medical School, Chinese PLA General Hospital, Beijing 100853, China. Tel: +86-15801607831; E-mail: meng6512@vip.sina.com

References

[1] Sung H, Ferlay J, Siegel RL, Laversanne M, Soerjomataram I, Jemal A and Bray F. Global cancer statistics 2020: GLOBOCAN estimates of incidence and mortality worldwide for 36 cancers in 185 countries. CA Cancer J Clin 2021; 71: 209-249.

[2] Ghobrial IM, Witzig TE and Adjei AA. Targeting apoptosis pathways in cancer therapy. CA Cancer J Clin 2005; 55: 178-194.

[3] Broz P, Pelegrin P and Shao F. The gasdermins, a protein family executing cell death and inflammation. Nat Rev Immunol 2020; 20: 143-157.

[4] Wang L, Li K, Lin X, Yao Z, Wang S, Xiong X, Ning Z, Wang J, Xu X, Jiang Y, Liu D, Chen Y, Zhang D and Zhang H. Metformin induces human esophageal carcinoma cell pyroptosis by targeting the miR-497/PELP1 axis. Cancer Lett 2019; 450: 22-31.

[5] Lu L, Zhang Y, Tan X, Merkher Y, Leonov S, Zhu L, Deng Y, Zhang H, Zhu D, Tan Y, Fu Y, Liu T and Chen Y. Emerging mechanisms of pyroptosis and its therapeutic strategy in cancer. Cell Death Discov 2022; 8: 338.

[6] Xiao Y, Zhang T, Ma X, Yang QC, Yang LL, Yang SC, Liang M, Xu Z and Sun ZJ. Microenvironment-responsive prodrug-induced pyroptosis boosts cancer immunotherapy. Adv Sci (Weinh) 2021; 8: e2101840.
[7] Tang R, Xu J, Zhang B, Liu J, Liang C, Hua J, Meng Q, Yu X and Shi S. Ferroptosis, necroptosis, and pyroptosis in anticancer immunity. J Hematol Oncol 2020; 13: 110.
[8] Lisio MA, Fu L, Goyeneche A, Gao ZH and Telleria C. High-grade serous ovarian cancer: basic sciences, clinical and therapeutic standpoints. Int J Mol Sci 2019; 20: 952.
[9] Goyeneche A, Lisio MA, Fu L, Srinivasan R, Valdez Capuccino J, Gao ZH and Telleria C. The capacity of high-grade serous ovarian cancer cells to form multicellular structures spontaneously along disease progression correlates with their orthotopic tumorigenicity in immunosuppressed mice. Cancers (Basel) 2020; 12: 699.
[10] Sadeghi N and Gerber DE. Targeting the PI3K pathway for cancer therapy. Future Med Chem 2012; 4: 1153-1169.
[11] Punt CJ, Boni J, Bruntsch U, Peters M and Thielert C. Phase I and pharmacokinetic study of CCI-779, a novel cytostatic cell-cycle inhibitor, in combination with 5-fluorouracil and leucovorin in patients with advanced solid tumors. Ann Oncol 2003; 14: 931-937.
[12] Bowtell DD, Bohm S, Ahmed AA, Aspuria PJ, Bast RC Jr, Beral V, Berek JS, Birrer MJ, Blagden S, Bookman MA, Brenton JD, Chiappinelli KB, Martins FC, Coukos G, Drapkin R, Edmondson R, Fotopoulou C, Gabra H, Galon J, Gourley C, Heong V, Huntsman DG, Iwanicki M, Karlan BY, Kaye A, Lengyel E, Levine DA, Lu KH, McNeish IA, Menon U, Narod SA, Nelson BH, Nephew KP, Pharoah P, Powell DJ Jr, Ramos P, Romero IL, Scott CL, Sood AK, Stronach EA and Balkwill FR. Rethinking ovarian cancer II: reducing mortality from high-grade serous ovarian cancer. Nat Rev Cancer 2015; 15: 668-679.
[13] Cook SA and Tinker AV. PARP inhibitors and the evolving landscape of ovarian cancer management: a review. BioDrugs 2019; 33: 255-273.
[14] Cortez AJ, Tudrej P, Kujawa KA and Lisowska KM. Advances in ovarian cancer therapy. Cancer Chemother Pharmacol 2018; 81: 17-38.
[15] Wang L, Qin X, Liang J and Ge P. Induction of pyroptosis: a promising strategy for cancer treatment. Front Oncol 2021; 11: 635774.
[16] Berkel C and Cacan E. Differential expression and copy number variation of gasdermin (GSDM) family members, pore-forming proteins in pyroptosis, in normal and malignant serous ovarian tissue. Inflammation 2021; 44: 2203-2216.
[17] Li J, Yang C, Li Y, Chen A, Li L and You Z. LncRNA GAS5 suppresses ovarian cancer by inducing inflammasome formation. Biosci Rep 2018; 38: BSR20171150.
[18] Tan C, Liu W, Zheng ZH and Wan XG. LncRNA HOTTIP inhibits cell pyroptosis by targeting miR-148a-3p/AKT2 axis in ovarian cancer. Cell Biol Int 2021; 45: 1487-1497.
[19] Qiao L, Wu X, Zhang J, Liu L, Sui X, Zhang R, Liu W, Shen F, Sun Y and Xi X. alpha-NETA induces pyroptosis of epithelial ovarian cancer cells through the GSDMD/caspase-4 pathway. FASEB J 2019; 33: 12760-12767.
[20] Liu T, Hou M, Li M, Qiu C, Cheng L, Zhu T, Qu J and Li L. Pyroptosis: a developing foreland of ovarian cancer treatment. Front Oncol 2022; 12: 828303.
[21] Zhang R, Chen J, Mao L, Guo Y, Hao Y, Deng Y, Han X, Li Q, Liao W and Yuan M. Nobiletin triggers reactive oxygen species-mediated pyroptosis through regulating autophagy in ovarian cancer cells. J Agric Food Chem 2020; 68: 1326-1336.
[22] Liang J, Zhou J, Xu Y, Huang X, Wang X, Huang W and Li H. Osthole inhibits ovarian carcinoma cells through LC3-mediated autophagy and GSDME-dependent pyroptosis except for apoptosis. Eur J Pharmacol 2020; 874: 172990.
[23] Dan HC, Sun M, Kaneko S, Feldman RI, Nicosia SV, Wang HG, Tsang BK and Cheng JQ. Akt phosphorylation and stabilization of X-linked inhibitor of apoptosis protein (XIAP). J Biol Chem 2016; 291: 22846.
[24] Ding S, Chamberlain M, McLaren A, Goh L, Duncan I and Wolf CR. Cross-talk between signalling pathways and the multidrug resistant protein MDR-1. Br J Cancer 2001; 85: 1175-1184.
[25] Cheng Q, Bao L, Li M, Chang K and Yi X. Erastin synergizes with cisplatin via ferroptosis to inhibit ovarian cancer growth in vitro and in vivo. J Obstet Gynaecol Res 2021; 47: 2481-2491.
[26] Tian W, Wang Z, Tang NN, Li JT, Liu Y, Chu WF and Yang BF. Ascorbic acid sensitizes colorectal carcinoma to the cytotoxicity of arsenic trioxide via promoting reactive oxygen species-dependent apoptosis and pyroptosis. Front Pharmacol 2020; 11: 123.
[27] Chen X, Dai X, Zou P, Chen W, Rajamanickam V, Feng C, Zhuge W, Qiu C, Ye Q, Zhang X and Liang G. Curcuminoid EF24 enhances the anti-tumour activity of Akt inhibitor MK-2206 through ROS-mediated endoplasmic reticulum stress and mitochondrial dysfunction in gastric cancer. Br J Pharmacol 2017; 174: 1131-1146.
[28] Li R, Jia Z and Trush MA. Defining ROS in biology and medicine. React Oxyg Species (Apex) 2016; 1: 9-21.
[29] Yi J, Zhu J, Wu J, Thompson CB and Jiang X. Oncogenic activation of PI3K-AKT-mTOR sig-

naling suppresses ferroptosis via SREBP-mediated lipogenesis. Proc Natl Acad Sci U S A 2020; 117: 31189-31197.
[30] Wang Y, Gao W, Shi X, Ding J, Liu W, He H, Wang K and Shao F. Chemotherapy drugs induce pyroptosis through caspase-3 cleavage of a gasdermin. Nature 2017; 547: 99-103.
[31] Rogers C, Fernandes-Alnemri T, Mayes L, Alnemri D, Cingolani G and Alnemri ES. Cleavage of DFNA5 by caspase-3 during apoptosis mediates progression to secondary necrotic/pyroptotic cell death. Nat Commun 2017; 8: 14128.
[32] Gao J, Qiu X, Xi G, Liu H, Zhang F, Lv T and Song Y. Downregulation of GSDMD attenuates tumor proliferation via the intrinsic mitochondrial apoptotic pathway and inhibition of EGFR/Akt signaling and predicts a good prognosis in non-small cell lung cancer. Oncol Rep 2018; 40: 1971-1984.
[33] Lin C and Zhang J. Inflammasomes in inflammation-induced cancer. Front Immunol 2017; 8: 271.
[34] Wu X, Mao X, Huang Y, Zhu Q, Guan J and Wu L. Detection of proteins associated with the pyroptosis signaling pathway in breast cancer tissues and their significance. Int J Clin Exp Pathol 2020; 13: 1408-1414.
[35] Wagner M, Roh V, Strehlen M, Laemmle A, Stroka D, Egger B, Trochsler M, Hunt KK, Candinas D and Vorburger SA. Effective treatment of advanced colorectal cancer by rapamycin and 5-FU/oxaliplatin monitored by TIMP-1. J Gastrointest Surg 2009; 13: 1781-1790.
[36] Derangere V, Chevriaux A, Courtaut F, Bruchard M, Berger H, Chalmin F, Causse SZ, Limagne E, Vegran F, Ladoire S, Simon B, Boireau W, Hichami A, Apetoh L, Mignot G, Ghiringhelli F and Rebe C. Liver X receptor beta activation induces pyroptosis of human and murine colon cancer cells. Cell Death Differ 2014; 21: 1914-1924.
[37] Lin CC and Chi JT. Ferroptosis of epithelial ovarian cancer: genetic determinants and therapeutic potential. Oncotarget 2020; 11: 3562-3570.

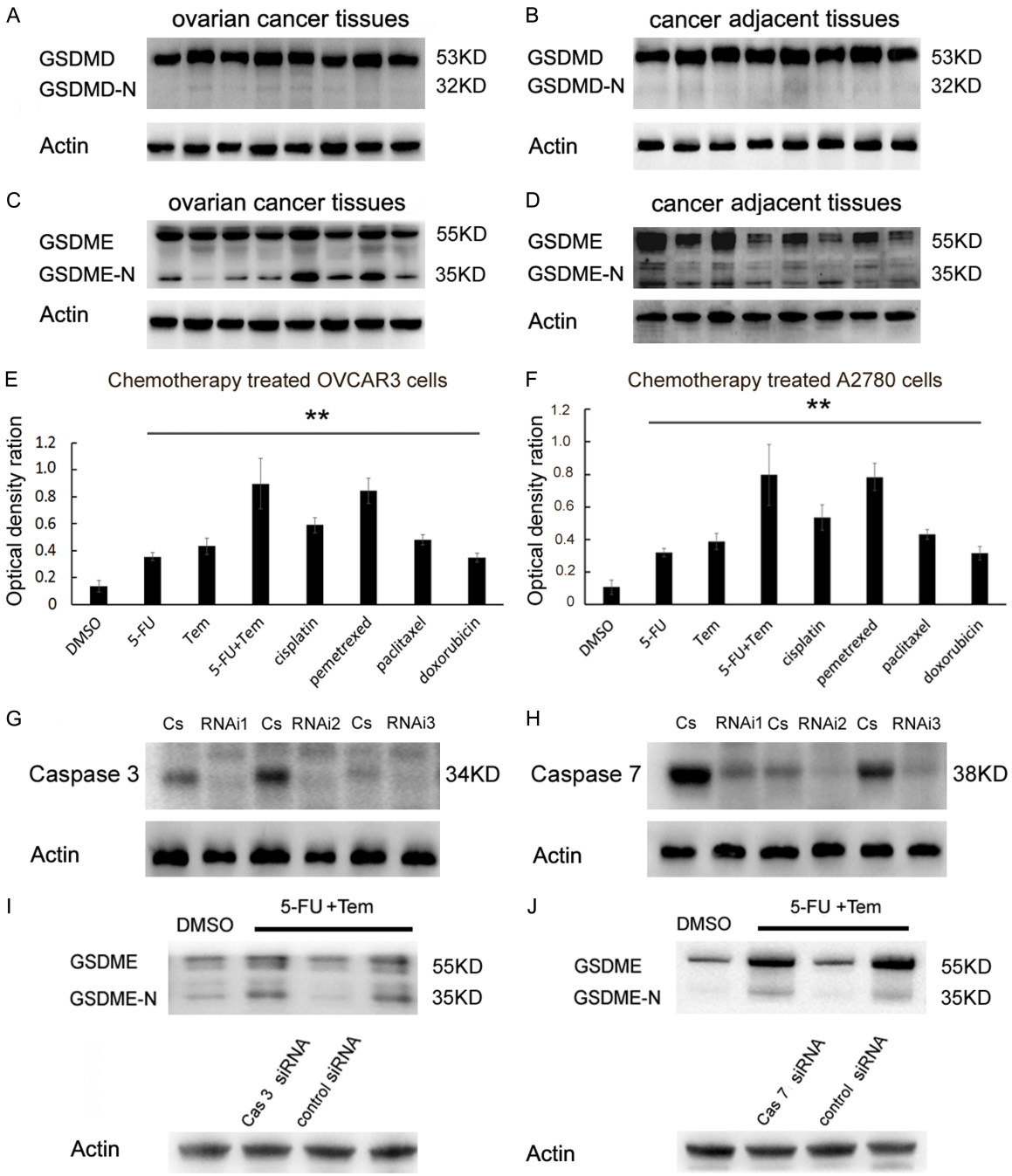

Supplementary Figure 1. GSDME mediated pyroptosis in chemotherapy treated ovarian cancer cells through caspase 3/7. (A-D) Analysis of eight additional ovarian cancer tissues and paired adjacent non-cancerous tissues. Full-length GSDMD was detected in both malignant and adjacent tissues, whike the activated GSDMD N-terminal fragment was absent in both (A, B). Full-length GSDME and its N-terminal fragment were detected in both tissue types, with cancer-specific accumulation of cleaved GSDME N-terminal (C, D). (E, F) Statistical analysis of Western blot data showed significantly increased GSDME N-terminal levels in A2780 and OVCAR3 cells following 48-hour chemotherapy treatments (5-FU, temsirolimus, 5-FU + temsirolimus, cisplatin, pemetrexed, paclitaxel, doxorubicin) as compared to DMSO controls. (G, H) OVCAR3 cells transfected with caspase-3/7 siRNAs exhibited robust protein knockdown, confirmed by Western blot. (I, J) Combined 5-FU and temsirolimus treatment resulted in markedly reduced GSDME N-terminal formation in caspase-3/7 knockdown cells compared to drug-treated control siRNA cells (**P < 0.01). Lanes: Untreated control, drug-treated control, drug + caspase-3/7 siRNA, drug + control siRNA (Cs).